Climate warming accelerates surface soil moisture drying in the Yellow River Basin, China

Keke Fan[1,2,3,4†], Louise Slater[4], Qiang Zhang[2,3,5*†], Justin Sheffield[6], Pierre Gentine[7], Shuai Sun[2,3,8], Wenhuan Wu[2,3,9]

1 College of Agronomy, Longzi Lake Campus, Henan Agricultural University, Zhengzhou, China

2 State Key Laboratory of Earth Surface Processes and Resource Ecology, Beijing Normal University, Beijing, China

3 Faculty of Geographical Science, Beijing Normal University, Beijing, China

4 School of Geography and the Environment, University of Oxford, Oxford, UK

5 Collaborative Innovation Center for Integrated Management of Water Resources and Water Environment in the Inner Mongolia Reaches of the Yellow River, Hohhot, China

6 Geography and Environment, University of Southampton, Southampton, UK

7 Department of Earth of Environmental Engineering, Columbia University, New York, USA

8 National Meteorological Information Center, China Meteorological Administration, Beijing, China

9 National Key Laboratory of Remote Sensing Information and Imagery Analyzing Technology, Beijing Research Institute of Uranium Geology, Beijing, China

***Corresponding author**: Prof. Dr. Qiang Zhang, zhangq68@bnu.edu.cn

[†]Keke Fan and Qiang Zhang contributed equally to this work.

Abstract: Understanding the dynamic response of surface soil moisture (SSM; 0-7 cm) drying to rising temperature is vital to predict future changes in agricultural and hydrological drought. Here we use quantile regression to explore the scaling effects of 2-m air temperature on SSM (%/°C) of the driest month in 8 different land cover types in the Yellow River Basin by using temperature intervals and a sliding window approach. SSM decreases significantly with air temperature and decreases more rapidly in warmer conditions, except for plain field, suggesting temperature has a greater effect on SSM-temperature scaling than land cover. For warmer conditions, scaling exhibits larger spatial heterogeneity, indicating that it is mainly affected by local factors. When SSM is moderate, the scaling is constrained by various factors, but mainly by temperature. Comparatively, the scaling is close to 0 when SSM is very high or very low. The study highlights that global warming effects on drought may be underestimated. The findings provide an important theoretical basis for the study of the effect of temperature on soil moisture and the prediction of droughts in the future.

Keywords: Surface soil moisture; Drought; Climate change; Temperature; Land cover; Quantile regression

1 Introduction

Drought is a frequently occurring extreme event caused by hydro-climatic deficit (Dai, 2011; Sheffield et al., 2008), with significant adverse effects on ecosystems,

hydrology, agriculture and economies globally (Liu et al., 2021; Vicente-Serrano et al., 2012). However, for many regions, the magnitude and even direction of climate warming-induced drought trends depends on how drought is defined, and there are often large differences between drought indicators used such as precipitation, soil moisture, runoff, and vegetation health (Brunner et al., 2021; Cook et al., 2018; Diffenbaugh et al., 2015). Even at the land surface, strong differences across drought indicators are evident (Cook et al., 2018).

The transition from meteorological drought (i.e., insufficient precipitation) to soil moisture drought depends on many processes that affect the surface water balance. Most importantly, however, soil moisture drought can be regarded as the time-integral balance between insufficient precipitation and subsequent loss of water including evapotranspiration, runoff and drainage (Berg & Sheffield, 2018; Cook et al., 2018). Soil moisture drought is crucial because reduced soil moisture is often related to soil water stress on vegetation, which limits the physiological functions of ecosystems, and thus can have significant impacts on agricultural production (Berg & Sheffield, 2018; Liu et al., 2021; Troch et al., 2013). Soil moisture, especially surface soil moisture (SSM), is also an important variable regulating the interaction between the land and the atmosphere (Fischer et al., 2007; Mishra, 2020; Guswa et al., 2002; Korres et al., 2014; Zhang et al., 2018) and can change the partitioning of water and energy fluxes (Trenberth et al., 2014).

The growing body of literature shows that climate warming might have increased historical soil moisture drought (Dai, 2013; Gu et al., 2019a and 2019b; Miralles et al.,

2019), and might also exacerbate the severity of future droughts, possibly even sharply (Berg et al., 2018). As noted above, based on multi-satellite datasets, a decrease of global SSM was observed in 1988-2010, with more regions showing negative trends (Dorigo et al., 2012). Comparatively, despite differences among climate models in the complexity of their surface components and large uncertainties in the simulated soil moisture fields, models can predict robust reductions in future SSM across most regions of the globe, with approximately 70% of the land area showing reductions in the multi-model mean SSM under the RCP8.5 scenario (Berg et al., 2017 and 2018; Cheng et al., 2017) and regional declines of up to 10% (Zhao and Dai, 2015; Cheng et al., 2017). Even in regions with increased precipitation, no regions show statistically significant increases of SSM in models (Berg & Sheffield, 2018). In contrast, changes of total-column soil moisture are more uncertain, with only slightly negative global mean, mostly in regions with decreased precipitation (Sheffield et al., 2008; Cook et al., 2018).

Consistently, different measurements of SSM drought suggest there will be spatially widespread increased drought in warmer climates, due to temperature-driven increases in evapotranspiration demand (Berg & Sheffield, 2018; Dorigo et al., 2012) The widespread SSM drying is significantly lower than the drying predicted from localized precipitation declines alone, suggesting that warming may be an important amplifier of soil moisture drought (Cook et al., 2018; Williams et al., 2015). For example, in most regions, warmer temperatures can exacerbate soil moisture drying by increasing evapotranspiration and reducing snowfall and snowpack levels despite uncertain precipitation changes (Cook et al., 2018). The rate of soil moisture drying

varies with the climatic characteristics, land cover, soil type, and drought severity (Fan et al., 2021; McColl et al., 2017; Tang and Piechota, 2009; Vicente-Serrano et al, 2020), For instance, land cover and soil type can influence drought by altering the surface partitioning of precipitation (e.g., interception, infiltration and runoff) and regulating water fluxes between the surface and the atmosphere (Fan et al., 2019; Cook et al., 2018). Previous studies have mainly focused on the long-term changes of soil moisture under the background of global warming, while in-depth research on the effect of rising temperature on soil moisture drought is lacking. Based on this, we proposed the following questions: what is the impact of rising temperature on SSM drought? Is the relationship linear? This will improve our understanding of the changes of soil moisture drought under climate change.

The Yellow River Basin is an ecologically fragile area in China and is extremely sensitive to climate warming (Li et al., 2019). Studies show that with global warming, soil moisture has become drier in the region (Wang et al., 2011), and such drying can significantly affect the ecological environment, especially the artificial ecological restoration implemented in recent years (Li et al., 2019). SSM in the driest month of each year was chosen to mitigate the influence of hydrological factors such as precipitation and groundwater, and because long-term SSM is more sensitive to rising temperature relative to total-column soil moisture (Sheffield et al., 2008; Whan et al., 2015), and because external water recharge by precipitation and groundwater is weak under drought conditions. Based on this, we used SSM of ERA5-Land in the driest

month of the year, with different temperature intervals and sliding windows, to explore the effect of rising temperature on SSM drought in 8 different vegetation land covers.

2 Data Sets and Methods

2.1 Data Sets

ERA5-Land is the fifth generation ECMWF (European Centre for Medium-Range Weather Forecasts), publicly-available, high-resolution (0.1°×0.1°) hourly reanalysis dataset produced by the Copernicus Climate Change Service (C3S), providing the possibility of detailed studies at the watershed scale (Muñoz Sabater, 2021). It also provides a consistent view of the evolution of land variables from 1981 to present, combining model data with observational data into a globally complete and consistent data set. ERA5-Land contains four soil layers (Layer 1: 0 -7 cm, Layer 2: 7-28 cm, Layer 3: 28-100 cm, Layer 4: 100-289 cm). ERA5-Land SSM (0-7 cm) dataset has been widely used and performs well in general when compared with observations and other model/satellite datasets (Beck et al., 2021; Muñoz Sabater et al., 2021).

For temperature, we use 2-meter air temperature data from the China Meteorological Forcing Dataset (CMFD), a set of near-surface meteorological and environmental reanalysis developed by the Institute of Tibetan Plateau Research, Chinese Academy of Sciences (He et al., 2020). CMFD merges a series of remote sensing datasets, reanalysis datasets and in-situ observation data, including GLDAS data (Rodell et al., 2004), MERRA pressure data (Rienecker et al., 2011), GEWEX-SRB radiation data (Pinker et al., 2003), TRMM satellite precipitation data

(Kummerow et al., 2000) and in-situ data from the China Meteorological Administration (CMA; He et al., 2020). It spans 1979 to 2018 with a time resolution of 3 hours and a horizontal resolution of 0.1°×0.1° (He et al., 2020; Yang et al., 2010). CMFD has become one of the most widely used climate data sets in China due to consistent quality and continuous spatio-temporal coverage (He et al., 2020).

The land cover data comes from the remote sensing monitoring data of China's 5-year land status programme of the Resource and Environmental Science and Data Center. It is completed with the support of several major scientific and technological projects of the Ministry of Science and Technology of China and the Chinese Academy of Sciences, and covers a long period of time (1990/1995/2000/2005/2010) and the entire country. This data set uses Landsat remote sensing images as the main data source and has been verified through manual visual interpretation (Liu et al., 2014). The spatial resolution of this freely available data is 1 km × 1 km. The data set divides land cover into 6 primary types and 25 secondary types. The primary types are cultivated land, wooded land, grassland, water area, construction land and unused land (Liu et al., 2014). All data sets used in this study have been listed in Table 1.

2.2 Methods

We compute the mean SSM and meteorological data for each month and select the lowest monthly SSM in each year, and the corresponding temperature. The five-year land cover data (1990/1995/2000/2005/2010) of the remote sensing monitoring database of China's land cover status is used to obtain the modal land cover for the

entire study period (1981-2018). All data are resampled to the same spatial resolution (0.1°×0.1°) using a bilinear interpolation, except land cover data by the mode interpolation. The baseline period of 1981-2018 shared by the meteorological and SSM datasets was selected. The Yellow River Basin (YRB) has a total of 8,593 grid cells, subdivided into 3 primary land cover types and 8 subtypes (Table 2; Figure 1), namely: dry farmland (mountain field: 2.61% of total area, hilly field: 12.03%, and plain field: 14.45%), wooded land (forested land: 5.30% and shrubland: 5.38%), and grassland (dense grassland: 8.91%, medium-density grassland: 26.08% and sparse grassland: 15.38 %). Other land covers with small area or accumulated water are not considered in this study.

For each land cover type, we employ quantile regression to analyze the scaling of the driest monthly SSM with temperature. Quantile regression estimates the linear relationship between a set of explanatory variables and the quantiles of the response (or target) variables (Koenker & Hallock, 2001). The calculation of the quantile regression estimator minimizes the asymmetrical absolute value residuals, and it is more robust to outliers than the least squares approach and is more reliable in estimating coefficients for non-normal distributions.

Given a series of data pairs (x_i, y_i) for $i = 1, \ldots, n$, the quantile regression model is as follows (Koenker & Hallock, 2001; Wasko & Sharma, 2014):

$$y_i = \beta_0^{(p)} + \beta_1^{(p)} \times \epsilon_i^{(p)} \quad (1)$$

where p is the quantile ($0<p<1$) and ϵ_i is the regression error with zero expectation. The parameters $\hat{\beta}_0^{(p)}$ and $\hat{\beta}_1^{(p)}$ are employed to minimize D:

$$D\left(\beta_0^{(p)}, \beta_1^{(p)}\right) = p\sum_{y_i \geq \beta_0^{(p)} + \beta_1^{(p)} x_i} \left| y_i - \beta_0^{(p)} - \beta_1^{(p)} x_i \right| + (1 - p)\sum_{y_i < \beta_0^{(p)} + \beta_1^{(p)} x_i} \left| y_i - \beta_0^{(p)} - \beta_1^{(p)} x_i \right| \quad (2)$$

In this study, x_i refers to temperature, y_i is SSM, $\beta_1^{(p)}$ is the slope of the fitted quantile regression. The scaling of SSM with temperature is calculated by dividing the slope by the multi-annual mean driest SSM in the baseline period of 1981-2018. We employ a bootstrap approach to calculate the significance level of quantile regression.

We explore the influence of temperature on the scaling by splitting the temperature range into two parts reflecting cooler and warmer conditions, by using a fixed threshold temperature of 14 ºC, which is the median value of all data pairs, and by using the median for each land cover. The influence of temperature on scaling is further explored by employing the median temperature in each grid cell to ensure a sufficient and similar number of sequence pairs in each temperature interval. Finally, we equally assess the change in the scaling of SSM with temperature for every degree increase in temperature, using a one degree sliding window. To ensure that there are 10 (n=1, 2, 3, … , 10) sliding windows between the lowest temperature (T_{min}) and highest temperature (T_{max}) of all data pairs, the window length ($L= T_{max} - T_{min} -n+1$) is determined. We choose n = 10 to provide a balance between the number of windows and the number of points required in each window.

3 Results and Discussion

3.1 Scaling of SSM with Temperature

SSM decreases with mean air temperature, and the 50^{th} percentile regression of SSM with temperature is significantly negative in all land cover types ($p < 0.05$; Figure 2). These findings support the well-known negative feedback of temperature on SSM (Cheng & Huang, 2016; Deng et al., 2020; Lakshmi et al., 2003; Oki & Kanae, 2006) but additionally highlight how the strength of the feedback varies with temperature and land cover types. Increasing temperature reduces SSM by increasing evapotranspiration (Pascolini-Campbell et al., 2021), but it may also increase precipitation (Lenderink & van Meijgaard, 2008). Because the increase in precipitation is limited by atmospheric radiative cooling, it increases at a much lower rate than the Clausius-Clapeyron rate (of increasing atmospheric water vapor with increasing temperature), namely 1 ~ 2 %/K versus 7 %/K for the slope of Clausius-Clapeyron (Allen and Ingram, 2002; Pendergrass and Hartmann, 2014; Berg and Sheffield, 2018). Conversely, Penman-Monteith potential evapotranspiration is expected to increase much faster than precipitation on land, by about 5 %/K, and more homogeneously (Fu and Feng, 2014; Scheff and Frierson, 2014). Increased vapor pressure deficit, which is exponentially responding to temperature, increases atmospheric demand but also reduces evapotranspiration through stomatal conductance stress (Massmann et al., 2019). Typically, as temperature increases, the growth rate of evapotranspiration exceeds that of precipitation, which may explain why the SSM decreases (Deng et al., 2020; Zhang et al., 2019). Increasing air temperature is also likely to increase extreme precipitation but reduce the occurrence of precipitation (Ma et al., 2015; Slater et al., 2021; Wang et al., 2020). The reduction of moderate and light rain further exacerbates the lack of SSM

and may lead to agricultural drought, especially in drought months. Even in regions where precipitation increased due to warming, no significant increases of SSM were found in models (Berg & Sheffield, 2018).

Moreover, SSM has a higher decrease rate with increasing temperature in dry farmland (mountain field and hilly field), except for plain field (-0.34 %/ ºC), followed by wooded land and grassland (Figure 2i). These differences in deceleration rate may relate to the land cover type, climatic conditions, and evapotranspiration (Deng et al., 2020). As a main driver of transpiration, higher leaf area index leads to higher transpiration in wooded land than grassland (Kleb and Wilson, 1997; James et al., 2003). For dry farmland, the deceleration rate of SSM with temperature is significantly ($p < 0.05$) lower in plain field (-0.34 %/ ºC) than mountain field (-0.76 %/ ºC) and hilly field (-0.95 %/ ºC), even though the temperature in plain field (temperature: 16.19 ºC) is slightly higher than mountain field (15.70 ºC) and close to hilly field (16.24 ºC). Plain field features a lower average SSM in the driest month (0.18 m^3/m^3) than mountain field (0.22 m^3/m^3) and hilly field (0.21 m^3/m^3; Figure 1c), which may limit the water available for evaporation. Mountain field and hilly field have high air temperature compared to other land covers, with sufficient energy for evapotranspiration, which may lead to rapid decreases in SSM with increasing temperature. For wooded land, the deceleration rate of SSM with temperature is similar in shrubland (-0.55 %/ ºC) and forested land (-0.58 %/ ºC) due to similar SSM and temperature. For dense grassland, the change of SSM with the increase of temperature is the slowest, at -0.28 %/ºC (temperature: -0.63 ºC; slope: -0.85×10^{-2} m^3m^{-3}/ºC; SSM: 0.34 m^3/m^3; mainly due to

the lowest temperature, despite having the highest SSM), followed by medium-density grassland (-0.49 %/ºC) and sparse grassland (-0.56 %/ºC) (Figure 1 and 2). SSM declines faster with temperature in the lower vegetation coverage, indicating that the grass land cover has a limited effect on the reduction of SSM by transpiration. Meanwhile grassland with higher temperature shows greater decline of SSM with temperature, indicating that the difference of air temperature is the main influencing factor (Figure 1 and 2) rather than SSM or vegetation coverage.

Different land cover types witness notable differences in the regression coefficients and significance levels of different quantiles (Figure 2 and 3). Overall, the middle quantiles (30^{th}, 50^{th} and 70^{th} percentiles) of SSM decrease significantly and faster with temperature in most land cover types (Figure 2). However, in the whole watershed, the scaling of low quantiles is significantly smaller than high quantiles ($p < 0.05$), that is, $scaling_{10th} < scaling_{30th} < scaling_{50th} < scaling_{70th} < scaling_{90\%}$, indicating that when SSM is lower, SSM reduces faster with temperature temporally (Figure 3).

3.2 Difference in scaling in cooler vs warmer conditions

To further study the change of SSM with air temperature across climate conditions (i.e. temperature ranges), we further analyzed the scaling of SSM with temperature in cooler and warmer conditions by three methods: using a fixed threshold (14 ℃ which is the median value of all data pairs; Figure 4 and S1); a statistical median in each grid cell (Figure 5) and a sliding window (Figure 6). In all land cover types, the change of

SSM with temperature features a greater rate of decrease in warmer conditions (Figure 4, 5 and 6), which is significant except for sparse grassland (Figure 4a). The results from the sliding window analysis also suggest that SSM decreases faster as the sliding window moves to the higher temperature range, which is generally consistent with Figure 4 and 6. Previous work found that in high temperature conditions, an abnormally high coupling between temperature and soil moisture may occur in areas with low soil moisture (Miralles et al., 2012; Schwingshackl et al, 2017). For grassland, the differences between median scalings in cooler or warmer conditions are relatively small: respectively -0.26 %/°C and -0.77 %/°C for dense grassland ($p < 0.0001$); -0.41 %/°C and -0.65 %/°C for medium-density grassland ($p < 0.01$); -0.52 %/°C and -0.79 %/°C for sparse grassland ($p > 0.05$), however, the scaling shows a larger variation range in the warmer conditions (Figure 4a; Table 3). For wooded land, SSM decreases significantly faster and exhibits larger variation in warmer conditions; the scalings are respectively -1.96 %/°C and -0.21 %/°C for shrubland; -1.87 %/°C and -0.21 %/°C for forested land (Figure 4a). The scaling shows small difference between shrubland and forested land regardless of the temperature, suggesting that different forest types do not substantially affect the scaling. In contrast, substantial differences in scaling are found between cooler and warmer conditions suggesting temperature range may play a critical role in the influence of temperature on scaling. For dry farmland, SSM decreases significantly faster in warmer than cooler conditions, but with a similar variation range, and the scalings are, respectively: -0.37 %/°C and -2.01 %/°C for mountain field; -0.13 %/°C and -0.58 %/°C for plain field; -0.88 %/°C and -1.45 %/°C for hilly field

(Figure 4a; Table 3). Meanwhile, there are large differences among the mountain, plain and hilly fields.

SSM generally declines with temperature in most areas with large spatial heterogeneity in both cooler and warmer conditions (Figure 4 and 5; Cheng & Huang, 2016; Wang et al., 2011). In the cooler conditions, the scaling exhibits less spatial heterogeneity, which is consistent with large-scale climate variables, such as, temperature (Figure 1, 3b and 5b), indicating that it is not greatly affected by local land cover and local heterogeneity in evapotranspiration. Moreover, the scaling is positive in the lower reaches of YRB close to the river channel (Figure 1, 3b and 5b). In warmer conditions, there is an evident spatial difference of the scaling with larger fluctuation range, suggesting it is more uncertain and mainly affected by local factors, such as land cover and soil properties. In particular, the area with positive scaling is consistent with the area with low SSM, indicating low SSM features notable scaling uncertainty, due to the lack of soil moisture available for evaporation (Figure 1b, 3c, S2c). These results further indicate that the scaling varies in different conditions and land cover has a greater effect on the scaling in warmer conditions than in cooler conditions.

Due to the spatial climatological differences within any single land cover type, the scaling of SSM with temperature also has different spatial characteristics (Lakshmi et al., 2003; Miralles et al., 2012; Zhou et al., 2021). This is explored in Figure 7, which shows that the scaling of different sites has a negative correlation with air temperature

across all land cover types, indicating that the SSM drying in warmer areas is faster with increasing temperature (Figure 7). However, the decreasing rate of the scaling differs slightly among different land cover types. For every degree of temperature increase, the change of the scaling is -0.027 %/℃, with a high adjusted R^2 value for all grassland types, and the change of the scaling with temperature is higher in the shrubland (-0.042 %/℃) and mountain field (-0.046 %/℃), consistent with Figure 4. The adjusted R^2 in each land cover type, except for plain field and hilly field, is considerable, indicating the scaling is closely correlated with temperature in the spatial domain.

3.3 The effect of SSM on scaling

We further explored the relationship of scaling with SSM further (Figure 8 and S5) and found the scaling is close to zero under conditions of high SSM (Figure 8), suggesting that when soil moisture is reduced by evapotranspiration, other water sources are replenished to offset the reduction (Seneviratne et al., 2010). When SSM reduces by evapotranspiration, other water sources, such as deeper soil moisture, mitigate some of the evaporation reduction, resulting in that SSM is in dynamic equilibrium, so the scaling is close to 0 and rarely affected by temperature and SSM under conditions of high SSM.

The scaling also reduces rapidly to 0 with decreasing SSM when SSM is below a lower critical value (Figure 8). The change of SSM with temperature is mainly restricted by SSM (Seneviratne et al., 2010) and its feedback on evapotranspiration,

which leads to a reduction in the magnitude of evaporation, then, the scaling rapidly reduces to 0 as SSM reduces, in cases where SSM is not either evaporated by external energy or absorbed by vegetation (Edlefsen & Anderson, 1943).

When SSM is moderate, between the smaller and upper critical values of SSM, the scaling changes strongly with SSM (Figure 8) and is affected by many climate and non-climate factors, but mainly restricted by temperature (Figure 8). These variables, especially temperature, play an important role in SSM drought mainly through the evapotranspiration process, so we cannot ignore that in the case of moderate soil moisture, energy and soil moisture regulations jointly limit the evapotranspiration rates, in turn affecting soil moisture content (Seneviratne et al., 2010).

Discussions

In this study, quantile regression was used to obtain robust scalings, and three methods were used to reduce the uncertainty of results. However, the research results still have certain uncertainties which are sourced mainly from but are not limited to: (1) Uncertainty of SSM data. Since it is difficult to obtain in-situ observed SSM data, this study adopted the SSM assimilation dataset of ERA5-Land, which has been widely verified and applied (Beck et al., 2020). The assimilation system reflects the land-atmosphere interactions and the connection and transformation of SSM and subsoil moisture (Hersbach et al., 2020; Muñoz Sabater et al., 2021). In contrast, remotely-sensed soil moisture can only reflect the SSM state (Beck et al., 2020), and may not

adequately reflect soil moisture changes due to deep-rooted vegetation through transpiration. (2) Uncertainty of land cover. Although good quality land cover data was used in this study (Liu et al., 2014), the land cover in this region has changed during the study period due to natural and anthropogenic factors (Li et al., 2019), which will inevitably lead to changes in the impact of temperature on SSM variations. (3) Inconsistency of data sources. The ERA5-Land assimilation system integrates observational data into the numerical dynamic model, and obtains the optimal solution of each variable through physical processes and equations (Muñoz Sabater et al., 2021), but this also brings certain systematic errors (Hersbach et al., 2020). By selecting high-quality datasets from different sources, this study alleviates systematic errors caused by using datasets from the same assimilation system, but also leads to some inconsistencies. Nonetheless, the consistency of the results obtained by different methods supports the reliability of the conclusions. This study sheds new light on impact of rising temperature on soil moisture drought and has guiding significance for future risk management of soil moisture drought.

Conclusions

This study employs quantile regression to explore the effects of temperature on SSM in 8 different land cover types based on three methods, i.e., fixed threshold temperature intervals, the median temperature in each grid cell, and a sliding window approach. The results from the different methods are consistent and all support the

conclusion that higher mean temperature accelerates SSM drying. In particular, the key findings are: In the Yellow River Basin, SSM declined more rapidly with temperature in warmer land covers, suggesting that, relative to land cover, temperature has a greater effect on the response of SSM to temperature. Higher temperature accelerates SSM drying, even across different covers. In warmer conditions, the response of SSM to temperature exhibits spatial heterogeneity and substantial variation, suggesting that it is more uncertain and mainly affected by local factors such as land cover and soil type. When SSM is moderate, the response of SSM to temperature changes with SSM is restricted by multiple factors, but mainly by temperature, i.e., through evapotranspiration. The response of SSM to temperature is weak when SSM is too high and too low, and the response is restricted by insufficient SSM for evapotranspiration in the latter case. This work deepens the understanding of the impacts of rising temperature on soil moisture drought, and may guide future agricultural and hydrological drought risk management under a warming climate.

Acknowledgements: This research has been financially supported by the Major Science and Technology Projects of Inner Mongolia Autonomous Region, Grant No. 2020ZD0009 and the China National Key R&D Program, Grant No. 2019YFA0606900. All authors declare no conflict of interest. Our cordial gratitude should also be extended to the editor, Prof. Dr. Emmanouil Anagnostou and Prof. Dr, Jesus Mateo, and anonymous reviewers for their professional and pertinent comments which are greatly helpful for further quality improvement of this manuscript.

References:

Allen, M.R., Ingram, W.J., 2002. Constraints on future changes in climate and the hydrologic cycle. Nature 419(6903), 228–232. https://doi.org/10.1038/nature01092

Beck, H.E., Pan, M., Miralles, D.G., Reichle, R.H., Dorigo, W.A., Hahn, S., Sheffield, J., Karthikeyan, L., Balsamo, G., Parinussa, R.M., van Dijk, A.I.J.M., Du, J., Kimball, J.S., Vergopolan, N., Wood, E.F., 2021. Evaluation of 18 satellite- and model-based soil moisture products using in situ measurements from 826 sensors. Hydrology and Earth System Sciences 25(1), 17–40. https://doi.org/10.5194/hess-25-17-2021

Berg, A., Findell, K., Lintner, B., Giannini, A., Seneviratne, S.I., van den Hurk, B., Lorenz, R., Pitman, A., Hagemann, S., Meier, A., Cheruy, F., Ducharne, A., Malyshev, S., Milly, P.C.D., 2016. Land–atmosphere feedbacks amplify aridity increase over land under global warming. Nature Climate Change 6(9), 869–874. https://doi.org/10.1038/nclimate3029

Berg, A., Sheffield, J., 2018. Climate Change and Drought: the Soil Moisture Perspective. Current Climate Change Reports 4(2), 180–191. https://doi.org/10.1007/s40641-018-0095-0

Berg, A., Sheffield, J., Milly, P.C.D., 2017. Divergent surface and total soil moisture projections under global warming. Geophysical Research Letters 44(1), 236–244. https://doi.org/10.1002/2016gl071921

Brunner, M.I., Slater, L., Tallaksen, L.M., Clark, M., 2021. Challenges in modeling and predicting floods and droughts: A review. WIREs Water 8(3), e1520. https://doi.org/10.1002/wat2.1520

Cheng, S., Huang, J., 2016. Enhanced soil moisture drying in transitional regions under a warming climate. Journal of Geophysical Research: Atmospheres 121(6), 2542–2555. https://doi.org/10.1002/2015jd024559

Cheng, S., Huang, J., Ji, F., Lin, L., 2017. Uncertainties of soil moisture in historical simulations and future projections. Journal of Geophysical Research: Atmospheres 122(4), 2239–2253. https://doi.org/10.1002/2016jd025871

Cook, B.I., Ault, T.R., Smerdon, J.E., 2015. Unprecedented 21st century drought risk in the American Southwest and Central Plains. Science Advances 1(1), e1400082. https://doi.org/10.1126/sciadv.1400082

Cook, B.I., Mankin, J.S., Anchukaitis, K.J., 2018. Climate Change and Drought: From Past to Future. Current Climate Change Reports 4(2), 164–179. https://doi.org/10.1007/s40641-018-0093-2

Dai, A., 2011. Characteristics and trends in various forms of the Palmer Drought Severity Index during 1900–2008. Journal of Geophysical Research 116, D12115. https://doi.org/10.1029/2010jd015541

Dai, A., 2012. Increasing drought under global warming in observations and models. Nature Climate Change 3(1), 52–58. https://doi.org/10.1038/nclimate1633

Deng, Y., Wang, S., Bai, X., Luo, G., Wu, L., Cao, Y., Li, H., Li, C., Yang, Y., Hu, Z., Tian, S., 2020. Variation trend of global soil moisture and its cause analysis. Ecological Indicators 110, 105939. https://doi.org/10.1016/j.ecolind.2019.105939

Diffenbaugh, N.S., Swain, D.L., Touma, D., 2015. Anthropogenic warming has increased drought risk in California. Proceedings of the National Academy of Sciences 112(13), 3931–3936. https://doi.org/10.1073/pnas.1422385112

Dorigo, W., de Jeu, R., Chung, D., Parinussa, R., Liu, Y., Wagner, W., Fernández-Prieto, D., 2012. Evaluating global trends (1988-2010) in harmonized multi-satellite surface soil moisture. Geophysical Research Letters 39(18), L18405. https://doi.org/10.1029/2012gl052988

Edlefsen, N.E., Anderson, A.B.C., 1943. Thermodynamics of soil moisture. Hilgardia 15(2), 31–298. https://doi.org/10.3733/hilg.v15n02p031

Fan, K., Zhang, Q., Li, J., Chen, D., Xu, C.-Y., 2021. The scenario-based variations and causes of future surface soil moisture across China in the twenty-first century. Environmental Research Letters 16(3), 034061. https://doi.org/10.1088/1748-9326/abde5e

Fan, K., Zhang, Q., Singh, V.P., Sun, P., Song, C., Zhu, X., Yu, H., Shen, Z., 2019. Spatiotemporal impact of soil moisture on air temperature across the Tibet Plateau. Science of The Total Environment 649, 1338–1348. https://doi.org/10.1016/j.scitotenv.2018.08.399

457 Fischer, E.M., Seneviratne, S.I., Vidale, P.L., Lüthi, D., Schär, C., 2007. Soil Moisture–
458 Atmosphere Interactions during the 2003 European Summer Heat Wave. Journal
459 of Climate 20(20), 5081–5099. https://doi.org/10.1175/jcli4288.1
460 Fu, Q., Feng, S., 2014. Responses of terrestrial aridity to global warming. Journal of
461 Geophysical Research: Atmospheres 119(13), 7863–7875.
462 https://doi.org/10.1002/2014jd021608
463 Gu, X., Zhang, Q., Li, J., Singh, V.P., Liu, J., Sun, P., Cheng, C., 2019a. Attribution of
464 Global Soil Moisture Drying to Human Activities: A Quantitative Viewpoint.
465 Geophysical Research Letters 46(5), 2573–2582.
466 https://doi.org/10.1029/2018gl080768
467 Gu, X., Zhang, Q., Li, J., Singh, V.P., Liu, J., Sun, P., He, C., Wu, J., 2019b.
468 Intensification and Expansion of Soil Moisture Drying in Warm Season Over
469 Eurasia Under Global Warming. Journal of Geophysical Research: Atmospheres
470 124(7), 3765–3782. https://doi.org/10.1029/2018jd029776
471 Guswa, A.J., Celia, M.A., Rodriguez-Iturbe, I., 2002. Models of soil moisture dynamics
472 in ecohydrology: A comparative study. Water Resources Research 38(9), 1166.
473 https://doi.org/10.1029/2001wr000826
474 He, J., Yang, K., Tang, W., Lu, H., Qin, J., Chen, Y., Li, X., 2020. The first high-
475 resolution meteorological forcing dataset for land process studies over China.
476 Scientific Data 7(1), 1–11. https://doi.org/10.1038/s41597-020-0369-y
477 Hersbach, H., Bell, B., Berrisford, P., Hirahara, S., Horányi, A., Muñoz-Sabater, J.,
478 Nicolas, J., Peubey, C., Radu, R., Schepers, D., Simmons, A., Soci, C., Abdalla,

S., Abellan, X., Balsamo, G., Bechtold, P., Biavati, G., Bidlot, J., Bonavita, M., Chiara, G., 2020. The ERA5 global reanalysis. Quarterly Journal of the Royal Meteorological Society 146(730), 1999–2049. https://doi.org/10.1002/qj.3803

Holsten, A., Vetter, T., Vohland, K., Krysanova, V., 2009. Impact of climate change on soil moisture dynamics in Brandenburg with a focus on nature conservation areas. Ecological Modelling 220(17), 2076–2087. https://doi.org/10.1016/j.ecolmodel.2009.04.038

Huang, J., Yu, H., Guan, X., Wang, G., Guo, R., 2015. Accelerated dryland expansion under climate change. Nature Climate Change 6(2), 166–171. https://doi.org/10.1038/nclimate2837

James, S.E., Pärtel, M., Wilson, S.D., Peltzer, D.A., 2003. Temporal heterogeneity of soil moisture in grassland and forest. Journal of Ecology 91(2), 234–239. https://doi.org/10.1046/j.1365-2745.2003.00758.x

Kleb, Heather R., Wilson, Scott D., 1997. Vegetation Effects on Soil Resource Heterogeneity in Prairie And Forest. The American Naturalist 150(3), 283–298. https://doi.org/10.1086/286066

Koenker, R., Hallock, K.F., 2001. Quantile Regression. Journal of Economic Perspectives 15(4), 143–156. https://doi.org/10.1257/jep.15.4.143

Korres, W., Reichenau, T.G., Schneider, K., 2013. Patterns and scaling properties of surface soil moisture in an agricultural landscape: An ecohydrological modeling study. Journal of Hydrology 498, 89–102. https://doi.org/10.1016/j.jhydrol.2013.05.050

Kummerow, C., Simpson, J., Thiele, O., Barnes, W., Chang, A.T.C., Stocker, E., Adler, R.F., Hou, A., Kakar, R., Wentz, F., Ashcroft, P., Kozu, T., Hong, Y., Okamoto, K., Iguchi, T., Kuroiwa, H., Im, E., Haddad, Z., Huffman, G., Ferrier, B., 2000. The Status of the Tropical Rainfall Measuring Mission (TRMM) after Two Years in Orbit. Journal of Applied Meteorology 39(12), 1965–1982. https://doi.org/2.0.co;2">10.1175/1520-0450(2001)040<1965:tsottr>2.0.co;2

Lakshmi, V., Jackson, T.J., Zehrfuhs, D., 2003. Soil moisture-temperature relationships: results from two field experiments. Hydrological Processes 17(15), 3041–3057. https://doi.org/10.1002/hyp.1275

Lenderink, G., van Meijgaard, E., 2008. Increase in hourly precipitation extremes beyond expectations from temperature changes. Nature Geoscience 1(8), 511–514. https://doi.org/10.1038/ngeo262

Li, J., Xie, S., Cook, E.R., Chen, F., Shi, J., Zhang, D.D., Fang, K., Gou, X., Li, T., Peng, J., Shi, S., Zhao, Y., 2019. Deciphering Human Contributions to Yellow River Flow Reductions and Downstream Drying Using Centuries-Long Tree Ring Records. Geophysical Research Letters 46(2), 898–905. https://doi.org/10.1029/2018gl081090

Liu, J., Kuang, W., Zhang, Z., Xu, X., Qin, Y., Ning, J., Zhou, W., Zhang, S., Li, R., Yan, C., Wu, S., Shi, X., Jiang, N., Yu, D., Pan, X., Chi, W., 2014. Spatiotemporal characteristics, patterns, and causes of land-use changes in China since the late 1980s. Journal of Geographical Sciences 24(2), 195–210. https://doi.org/10.1007/s11442-014-1082-6

Liu, Y., Liu, Y., Wang, W., Zhou, H., 2021. Propagation of soil moisture droughts in a hotspot region: Spatial pattern and temporal trajectory. Journal of Hydrology 593, 125906. https://doi.org/10.1016/j.jhydrol.2020.125906

Ma, S., Zhou, T., Dai, A., Han, Z., 2015. Observed Changes in the Distributions of Daily Precipitation Frequency and Amount over China from 1960 to 2013. Journal of Climate 28(17), 6960–6978. https://doi.org/10.1175/jcli-d-15-0011.1

Massmann, A., Gentine, P., Lin, C., 2019. When Does Vapor Pressure Deficit Drive or Reduce Evapotranspiration? Journal of Advances in Modeling Earth Systems 11(10), 3305–3320. https://doi.org/10.1029/2019ms001790

McColl, K.A., Alemohammad, S.H., Akbar, R., Konings, A.G., Yueh, S., Entekhabi, D., 2017. The global distribution and dynamics of surface soil moisture. Nature Geoscience 10(2), 100–104. https://doi.org/10.1038/ngeo2868

Miralles, D.G., Gentine, P., Seneviratne, S.I., Teuling, A.J., 2018. Land-atmospheric feedbacks during droughts and heatwaves: state of the science and current challenges. Annals of the New York Academy of Sciences 1436(1), 19–35. https://doi.org/10.1111/nyas.13912

Miralles, D.G., van den Berg, M.J., Teuling, A.J., de Jeu, R.A.M., 2012. Soil moisture-temperature coupling: A multiscale observational analysis. Geophysical Research Letters 39, L21707. https://doi.org/10.1029/2012gl053703

Mishra, V., 2020. Relative Contribution of Precipitation and Air Temperature on Dry Season Drying in India, 1951–2018. Journal of Geophysical Research: Atmospheres 125(15). https://doi.org/10.1029/2020jd032998

545 Muñoz-Sabater, J., Dutra, E., Agustí-Panareda, A., Albergel, C., Arduini, G., Balsamo,
546 G., Boussetta, S., Choulga, M., Harrigan, S., Hersbach, H., Martens, B., Miralles,
547 D.G., Piles, M., Rodríguez-Fernández, N.J., Zsoter, E., Buontempo, C., Thépaut,
548 J.-N., 2021. ERA5-Land: a state-of-the-art global reanalysis dataset for land
549 applications. Earth System Science Data 13, 4349–4383.
550 https://doi.org/10.5194/essd-13-4349-2021
551 Oki, T., 2006. Global Hydrological Cycles and World Water Resources. Science
552 313(5790), 1068–1072. https://doi.org/10.1126/science.1128845
553 Pascolini-Campbell, M., Reager, J.T., Chandanpurkar, H.A., Rodell, M., 2021. A 10
554 per cent increase in global land evapotranspiration from 2003 to 2019. Nature
555 593(7860), 543–547. https://doi.org/10.1038/s41586-021-03503-5
556 Pendergrass, A.G., Hartmann, D.L., 2014. The Atmospheric Energy Constraint on
557 Global-Mean Precipitation Change. Journal of Climate 27(2), 757–768.
558 https://doi.org/10.1175/jcli-d-13-00163.1
559 Pinker, R.T., Tarpley, J.D., Laszlo, I., Mitchell, K.E., Houser, P.R., Wood, E.F.,
560 Schaake, J.C., Robock, A., Lohmann, D., Cosgrove, B.A., Sheffield, J., Duan, Q.,
561 Luo, L., Higgins, R.W., 2003. Surface radiation budgets in support of the GEWEX
562 Continental-Scale International Project (GCIP) and the GEWEX Americas
563 Prediction Project (GAPP), including the North American Land Data Assimilation
564 System (NLDAS) project. Journal of Geophysical Research: Atmospheres
565 108(D22), 8844. https://doi.org/10.1029/2002jd003301

566 Rasmijn, L.M., van der Schrier, G., Bintanja, R., Barkmeijer, J., Sterl, A., Hazeleger,
567 W., 2018. Future equivalent of 2010 Russian heatwave intensified by weakening
568 soil moisture constraints. Nature Climate Change 8(5), 381–385.
569 https://doi.org/10.1038/s41558-018-0114-0
570 Rienecker, M.M., Suarez, M.J., Gelaro, R., Todling, R., Bacmeister, J., Liu, E.,
571 Bosilovich, M.G., Schubert, S.D., Takacs, L., Kim, G.-K., Bloom, S., Chen, J.,
572 Collins, D., Conaty, A., da Silva, A., Gu, W., Joiner, J., Koster, R.D., Lucchesi,
573 R., Molod, A., 2011. MERRA: NASA's Modern-Era Retrospective Analysis for
574 Research and Applications. Journal of Climate 24(14), 3624–3648.
575 https://doi.org/10.1175/jcli-d-11-00015.1
576 Rodell, M., Houser, P.R., Jambor, U., Gottschalck, J., Mitchell, K., Meng, C.-J. .,
577 Arsenault, K., Cosgrove, B., Radakovich, J., Bosilovich, M., Entin, J.K., Walker,
578 J.P., Lohmann, D., Toll, D., 2004. The Global Land Data Assimilation System.
579 Bulletin of the American Meteorological Society 85(3), 381–394.
580 https://doi.org/10.1175/BAMS-85-3-381
581 Scheff, J., Frierson, D.M.W., 2014. Scaling Potential Evapotranspiration with
582 Greenhouse Warming. Journal of Climate 27(4), 1539–1558.
583 https://doi.org/10.1175/jcli-d-13-00233.1
584 Schwingshackl, C., Hirschi, M., Seneviratne, S.I., 2017. Quantifying Spatiotemporal
585 Variations of Soil Moisture Control on Surface Energy Balance and Near-Surface
586 Air Temperature. Journal of Climate 30(18), 7105–7124.
587 https://doi.org/10.1175/jcli-d-16-0727.1

588 Seneviratne, S.I., Corti, T., Davin, E.L., Hirschi, M., Jaeger, E.B., Lehner, I., Orlowsky,
589 B., Teuling, A.J., 2010. Investigating soil moisture–climate interactions in a
590 changing climate: A review. Earth-Science Reviews 99(3-4), 125–161.
591 https://doi.org/10.1016/j.earscirev.2010.02.004
592 Sheffield, J., Wood, E.F., 2007. Projected changes in drought occurrence under future
593 global warming from multi-model, multi-scenario, IPCC AR4 simulations.
594 Climate Dynamics 31(1), 79–105. https://doi.org/10.1007/s00382-007-0340-z
595 Slater, L.J., Anderson, B., Buechel, M., Dadson, S., Han, S., Harrigan, S., Kelder, T.,
596 Kowal, K., Lees, T., Matthews, T., Murphy, C., Wilby, R.L., 2021. Nonstationary
597 weather and water extremes: a review of methods for their detection, attribution,
598 and management. Hydrology and Earth System Sciences 25, 3897–3935.
599 https://doi.org/10.5194/hess-25-3897-2021
600 Sousa, P.M., Barriopedro, D., García-Herrera, R., Ordóñez, C., Soares, P.M.M., Trigo,
601 R.M., 2020. Distinct influences of large-scale circulation and regional feedbacks
602 in two exceptional 2019 European heatwaves. Communications Earth &
603 Environment 1(1), 1-13. https://doi.org/10.1038/s43247-020-00048-9
604 Stéfanon, M., Drobinski, P., D'Andrea, F., Lebeaupin-Brossier, C., Bastin, S., 2013.
605 Soil moisture-temperature feedbacks at meso-scale during summer heat waves
606 over Western Europe. Climate Dynamics 42(3-4), 1309–1324.
607 https://doi.org/10.1007/s00382-013-1794-9

608 Tang, C., Piechota, T.C., 2009. Spatial and temporal soil moisture and drought
609 variability in the Upper Colorado River Basin. Journal of Hydrology 379(1-2),
610 122–135. https://doi.org/10.1016/j.jhydrol.2009.09.052
611 Trenberth, K.E., Dai, A., van der Schrier, G., Jones, P.D., Barichivich, J., Briffa, K.R.,
612 Sheffield, J., 2013. Global warming and changes in drought. Nature Climate
613 Change 4(1), 17–22. https://doi.org/10.1038/nclimate2067
614 Troch, P.A., Carrillo, G., Sivapalan, M., Wagener, T., Sawicz, K., 2013. Climate-
615 vegetation-soil interactions and long-term hydrologic partitioning: signatures of
616 catchment co-evolution. Hydrology and Earth System Sciences 17(6), 2209–2217.
617 https://doi.org/10.5194/hess-17-2209-2013
618 Vicente-Serrano, S.M., Beguería, S., Lorenzo-Lacruz, J., Camarero, J.J., López-
619 Moreno, J.I., Azorin-Molina, C., Revuelto, J., Morán-Tejeda, E., Sanchez-
620 Lorenzo, A., 2012. Performance of Drought Indices for Ecological, Agricultural,
621 and Hydrological Applications. Earth Interactions 16(10), 1–27.
622 https://doi.org/10.1175/2012ei000434.1
623 Vicente-Serrano, S.M., Quiring, S.M., Pena-Gallardo, M., Yuan, S., Dominguez-Castro,
624 F., 2020. A review of environmental droughts: Increased risk under global
625 warming? Earth-Science Reviews 201, 102953.
626 https://doi.org/10.1016/j.earscirev.2019.102953
627 Wang, A., Lettenmaier, D.P., Sheffield, J., 2011. Soil Moisture Drought in China,
628 1950–2006. Journal of Climate 24(13), 3257–3271.
629 https://doi.org/10.1175/2011jcli3733.1

Wang, G., Zhang, Q., Yu, H., Shen, Z., Sun, P., 2020. Double increase in precipitation extremes across China in a 1.5 °C/2.0 °C warmer climate. Science of The Total Environment 746, 140807. https://doi.org/10.1016/j.scitotenv.2020.140807

Wang, S., Zhang, Z., McVicar, T.R., Zhang, J., Zhu, J., Guo, J., 2012. An event-based approach to understanding the hydrological impacts of different land uses in semi-arid catchments. Journal of Hydrology 416, 50–59. https://doi.org/10.1016/j.jhydrol.2011.11.035

Wasko, C., Sharma, A., 2014. Quantile regression for investigating scaling of extreme precipitation with temperature. Water Resources Research 50(4), 3608–3614. https://doi.org/10.1002/2013wr015194

Whan, K., Zscheischler, J., Orth, R., Shongwe, M., Rahimi, M., Asare, E.O., Seneviratne, S.I., 2015. Impact of soil moisture on extreme maximum temperatures in Europe. Weather and Climate Extremes 9, 57–67. https://doi.org/10.1016/j.wace.2015.05.001

Williams, A.P., Seager, R., Abatzoglou, J.T., Cook, B.I., Smerdon, J.E., Cook, E.R., 2015. Contribution of anthropogenic warming to California drought during 2012–2014. Geophysical Research Letters 42(16), 6819–6828. https://doi.org/10.1002/2015gl064924

Yang, K., He, J., Tang, W., Qin, J., Cheng, C.C.K., 2010. On downward shortwave and longwave radiations over high altitude regions: Observation and modeling in the Tibetan Plateau. Agricultural and Forest Meteorology 150(1), 38–46. https://doi.org/10.1016/j.agrformet.2009.08.004

652 Zhang, Q., Fan, K., Singh, V.P., Song, C., Xu, C.-Y., Sun, P., 2019. Is Himalayan-
653 Tibetan Plateau “drying”? Historical estimations and future trends of surface soil
654 moisture. Science of The Total Environment 658, 374–384.
655 https://doi.org/10.1016/j.scitotenv.2018.12.209
656 Zhang, Q., Fan, K., Singh, V.P., Sun, P., Shi, P., 2018. Evaluation of Remotely Sensed
657 and Reanalysis Soil Moisture Against In Situ Observations on the Himalayan-
658 Tibetan Plateau. Journal of Geophysical Research: Atmospheres 123(14), 7132–
659 7148. https://doi.org/10.1029/2017jd027763
660 Zhao, T., Dai, A., 2015. The Magnitude and Causes of Global Drought Changes in the
661 Twenty-First Century under a Low–Moderate Emissions Scenario. Journal of
662 Climate 28(11), 4490–4512. https://doi.org/10.1175/jcli-d-14-00363.1
663 Zhou, S., Williams, A.P., Lintner, B.R., Berg, A.M., Zhang, Y., Keenan, T.F., Cook,
664 B.I., Hagemann, S., Seneviratne, S.I., Gentine, P., 2021. Soil moisture–
665 atmosphere feedbacks mitigate declining water availability in drylands. Nature
666 Climate Change 11(1), 38–44. https://doi.org/10.1038/s41558-020-00945-z

667 Table 1. The information and source of the datasets employed.

668

Dataset	Variable	Spatial resolution	Temporal resolution	Time range	Source
ERA5-Land	Surface soil moisture (0-7 cm)	0.1°×0.1°	hourly	1981-present	https://cds.climate.copernicus.eu
China meteorological forcing dataset	2-meter air temperature	0.1°×0.1°	daily	1979-2018	https://data.tpdc.ac.cn
Remote sensing monitoring data of China's land cover	Land cover	1 km × 1 km	5 years	1990/1995/2000/2005/2010/2015	http://www.resdc.cn

669

670 Table 2. Detailed information of land cover used in this study. The number of grid cells and the area
671 ratio of each land cover to the entire study area are provided. The land covers with open water or
672 small area ratio are not considered.
673

Primary classification	Second classification	Notes[b] (Area ratios; grid cells)
Dry farmland	Mountain field	(2.61%; 224)
	Hilly field	(12.03%; 1034)
	Plain field	(14.45%; 1242)
Wooded land	Forested land	Natural forests and plantations with a canopy density greater than 30%. (5.30%; 455)
	Shrubland	Low woodland and shrubland with a canopy density greater than 40% and a height of less than 2 meters. (5.38%; 462)
Grassland	Dense grassland	Grassland with a canopy density greater than 50%. (8.91%; 765)
	Medium-density grassland	Grassland with a canopy density of 20~50%. (26.08%; 2241)
	Sparse grassland	Grassland with a canopy density of 5-20%. (15.38%; 1322)

674

675 Table 3. The 25%, 50% and 75% percentile scalings for different temperature ranges (< 14 ℃, all
676 data and >= 14 ℃) in the eight different land covers which correspond to Figure 3.
677

	< 14 ℃			All data			>= 14 ℃		
	25%	50%	75%	25%	50%	75%	25%	50%	75%
Dense grassland	-0.49	-0.26	-0.16	-0.54	-0.28	-0.18	-1.92	-0.77	0.03
Medium-density grassland	-0.91	-0.41	-0.15	-0.91	-0.49	-0.18	-1.77	-0.65	0.29
Sparse grassland	-1.12	-0.52	-0.17	-1.06	-0.56	-0.24	-2.60	-0.79	0.60
Shrubland	-0.57	-0.21	0.02	-1.00	-0.55	-0.19	-3.06	-1.96	-0.53
Forested land	-0.55	-0.21	0.55	-1.10	-0.58	-0.23	-3.21	-1.87	-0.23
Mountain field	-0.64	-0.37	-0.01	-1.22	-0.76	-0.47	-2.81	-2.01	-1.17
Plain field	-0.59	-0.13	0.55	-0.69	-0.34	-0.10	-1.63	-0.58	0.13
Hilly field	-1.36	-0.88	-0.02	-1.28	-0.95	-0.58	-2.32	-1.45	-0.30

678

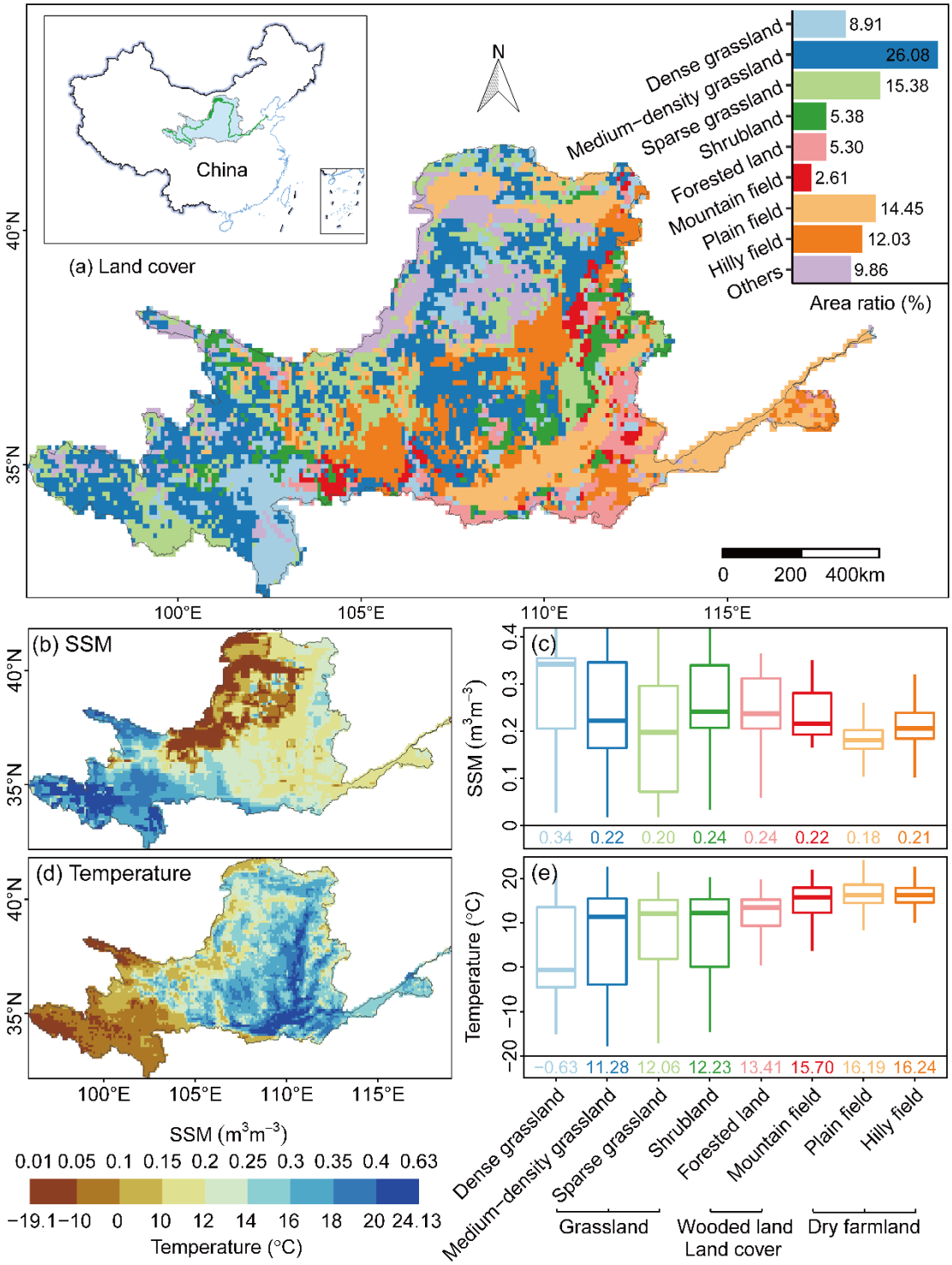

Figure 1. Land cover (a), the multi-annual average driest monthly surface soil moisture (hereafter: SSM; b-c), and corresponding 2-meter air temperature (Hereafter: Temperature; d-e) in the Yellow River Basin (0.1°×0.1°). The area ratios of different land cover types within the basin are provided (a). The land covers are ordered by the median temperature. The colored labels indicate the boxplot medians in different land covers (c and e). Kruskal Wallis test results are highly significant for both SSM and temperature across different land cover types ($p<0.001$).

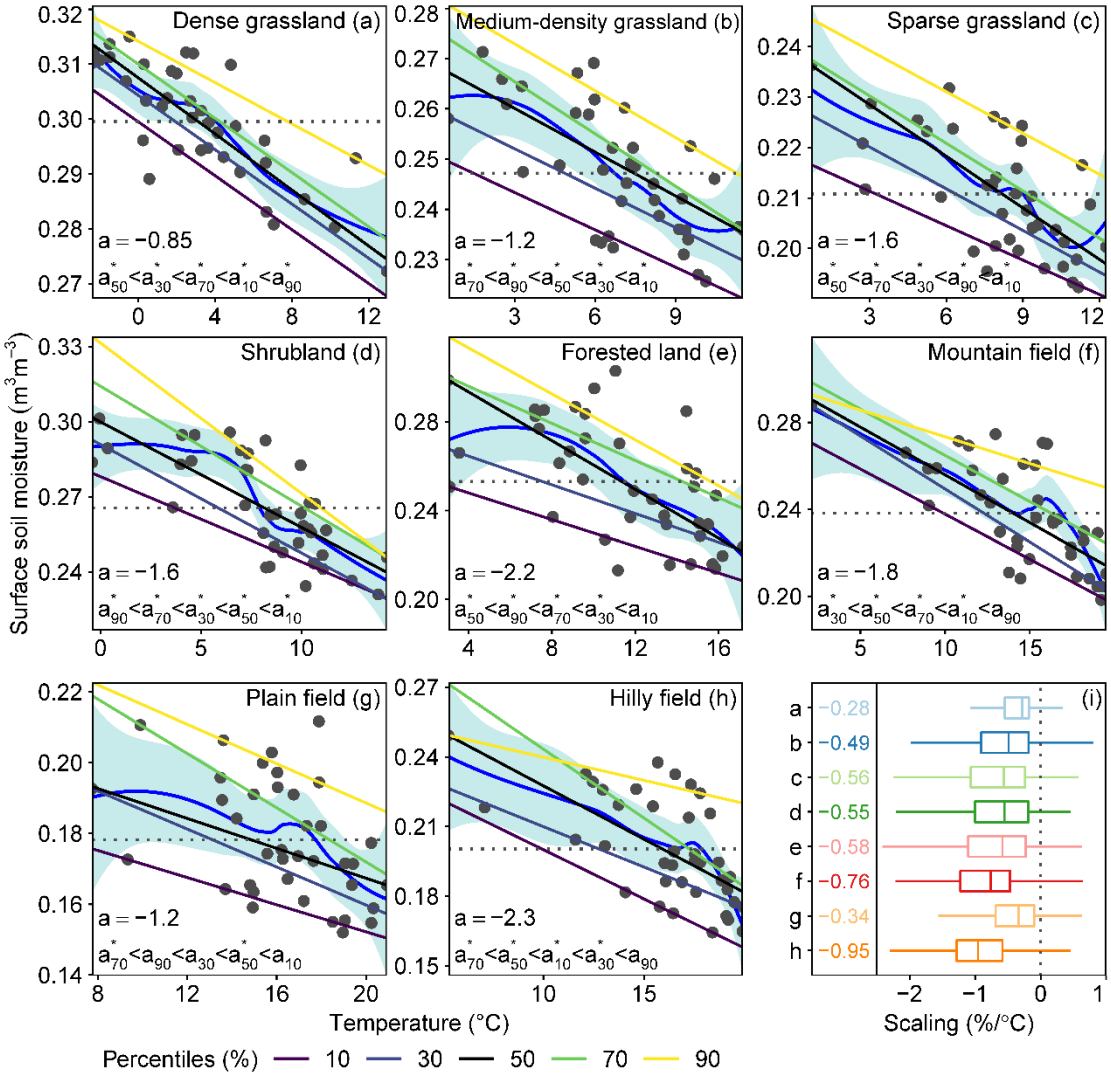

Figure 2. The relationship between SSM and temperature in different land cover types. The different oblique straight lines indicate the 10%, 30%, 50%, 70% and 90% quantile regression fits. The smooth blue curve and shading indicate the local polynomial regression fitting line and its 95% confidence interval. On each panel, the 50th percentile quantile regression coefficient ($10^{-2}m^3m^{-3}/^oC$) is provided, multiplied by 10^2. All quantile regression coefficients for all land cover types are negative. Regression coefficients with a superscript asterisk (*) are significant at the 95% level. The dashed horizontal lines indicate the mean SSM (a-h). The colored labels indicate the boxplot medians in different land covers (i); colors are the same as in Figure 1. The Kruskal Wallis test result for scaling across all land cover types is highly significant ($p<0.001$).

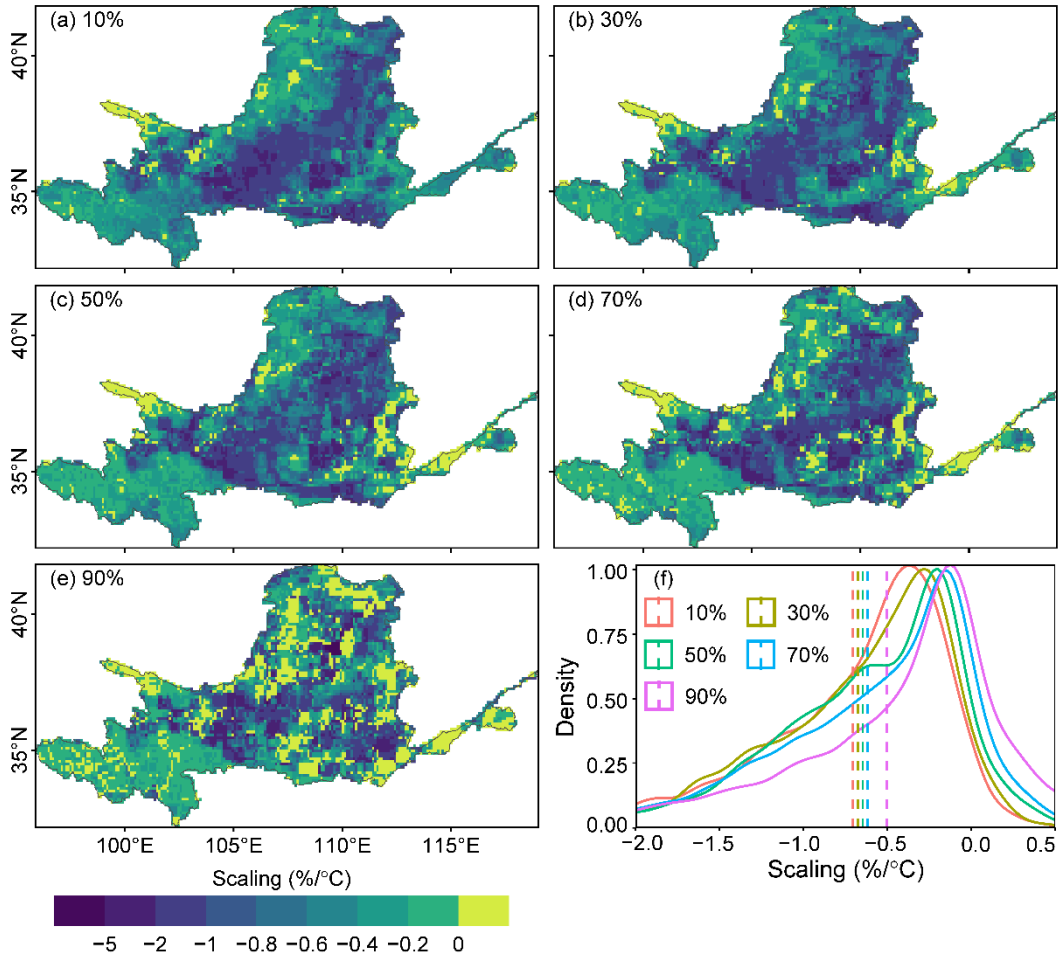

Figure 3. The spatial patterns (a-e) and the density curves (f) of scaling for different quantile regression of SSM with temperature. The 10%, 30%, 50%, 70% and 90% quantile regression scalings are provided corresponding to Figure 2. The p-value of Kruskal Wallis test for scalings across all quantiles and Wilcoxon test between pairwise groups are all far less than 0.

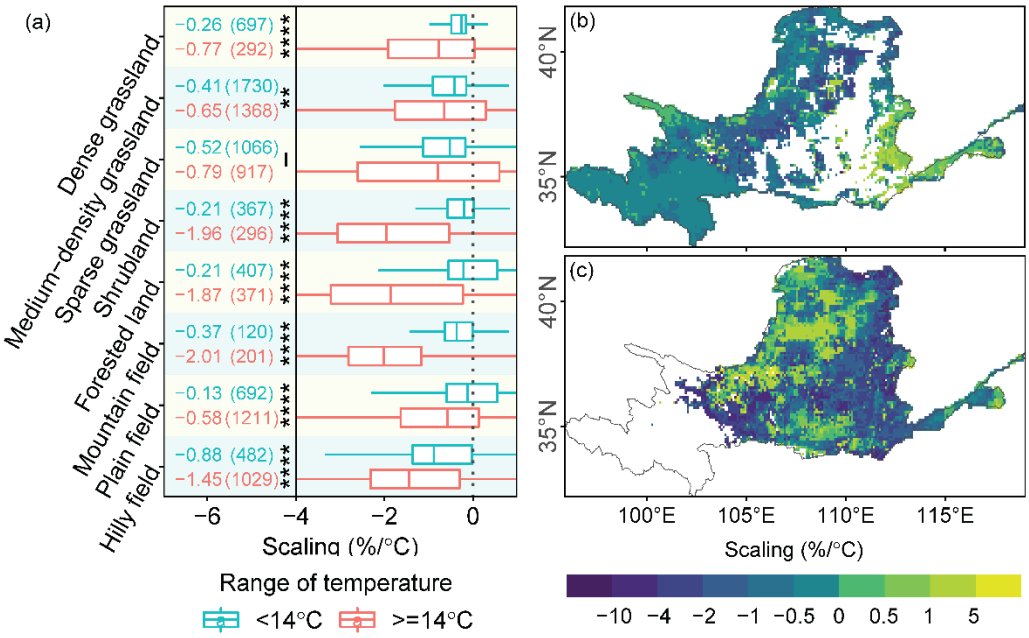

Figure 4. Scalings of SSM with temperature (%/°C) for the 50th percentile of quantile regression (panel a). Maps indicate scalings for temperature intervals of (b) less than 14 ºC, and (c) more than 14 ºC (which is close to the central temperature of all data used). Panel (a) zooms in on the boxplots for clarity (the full temperature interval is shown in Figure S1). The colored labels indicate the median and number (enclosed in parentheses) of scaling coefficients in each land cover type (a). The scaling is calculated only in grid cells with at least 10 data point pairs. The Kruskal Wallis test results for scalings in different temperature intervals have been provided in panel (a): "-", "*", "**", "***" and "****" respectively refer to p-values: >= 0.05, < 0.05, < 0.01, < 0.001 and < 0.0001. Moreover, the Kruskal Wallis test result for scalings across all land cover types is highly significant (p<0.001) in each temperature interval.

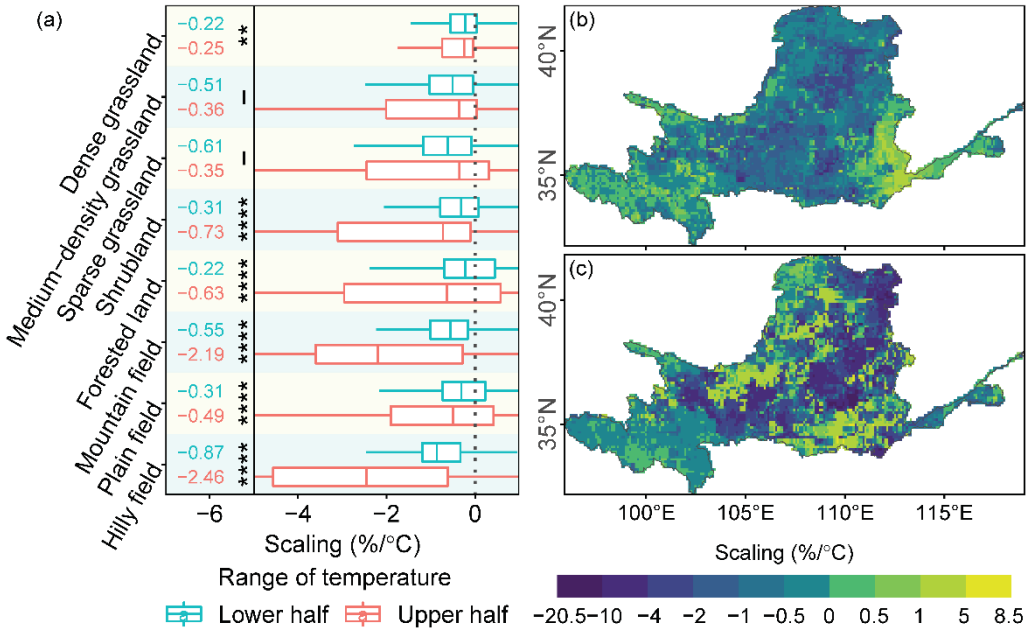

Figure 5. Scalings of SSM with temperature for the 50% quantile regression (panel a). Maps indicate (b) the lower half (0%-50%), and (c) the upper half (50%-100%) of the temperature range in each grid cell. Panel (a) zooms in on the boxplots for clarity. The colored labels indicate the median of scalings in different land covers in panel (a). The Kruskal Wallis test results for scalings in different temperature ranges have been provided in panel (a): "-", "*", "**", "***" and "****" respectively refer to the p-value: >= 0.05, < 0.05, < 0.01, < 0.001 and < 0.0001. Moreover, the p-value of Kruskal Wallis test for scalings across all land covers is < 0.0001 in each temperature range.

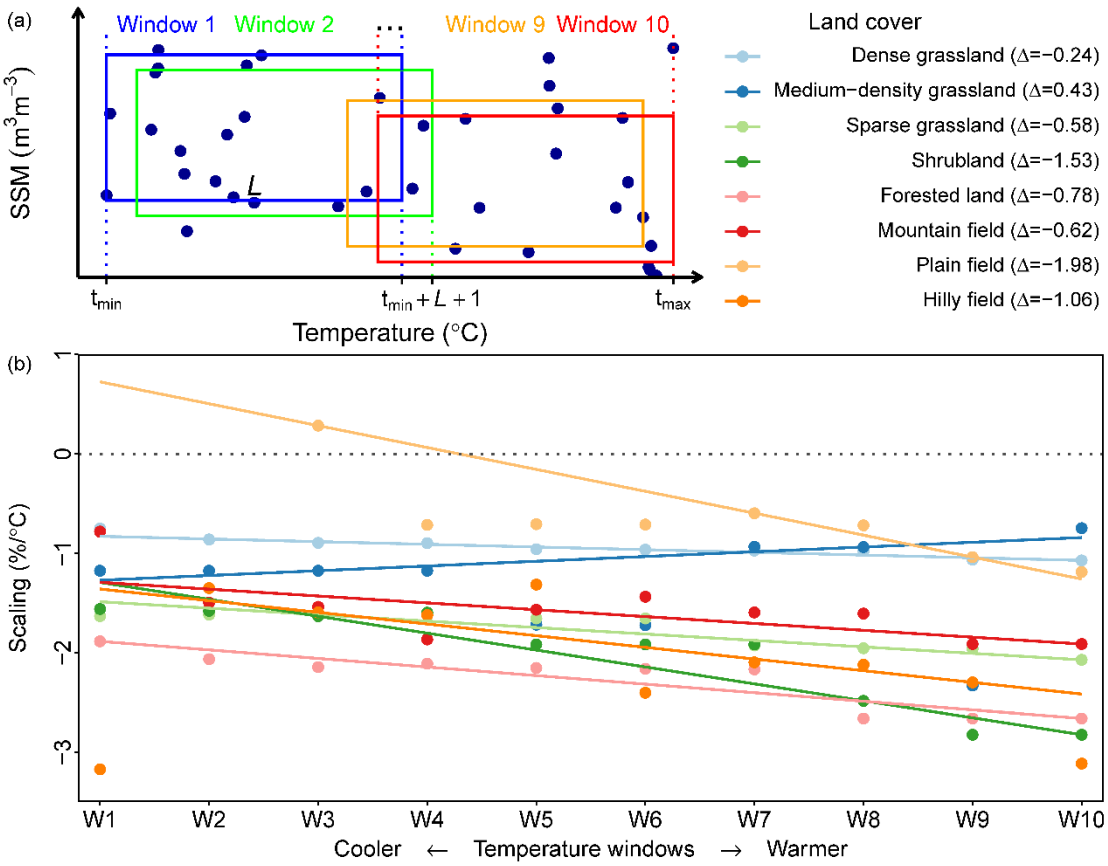

Figure 6. Scalings of SSM vs. temperature in different sliding windows. (a) shows the sliding window approach; (b) colored lines show the fitted line of 50% quantile regression of scaling with each window in different land cover types. The top right panel indicates the scaling change (Δ) under the sliding temperature window, which is derived by subtracting the fitted value of W1 from the fitted value of W10.

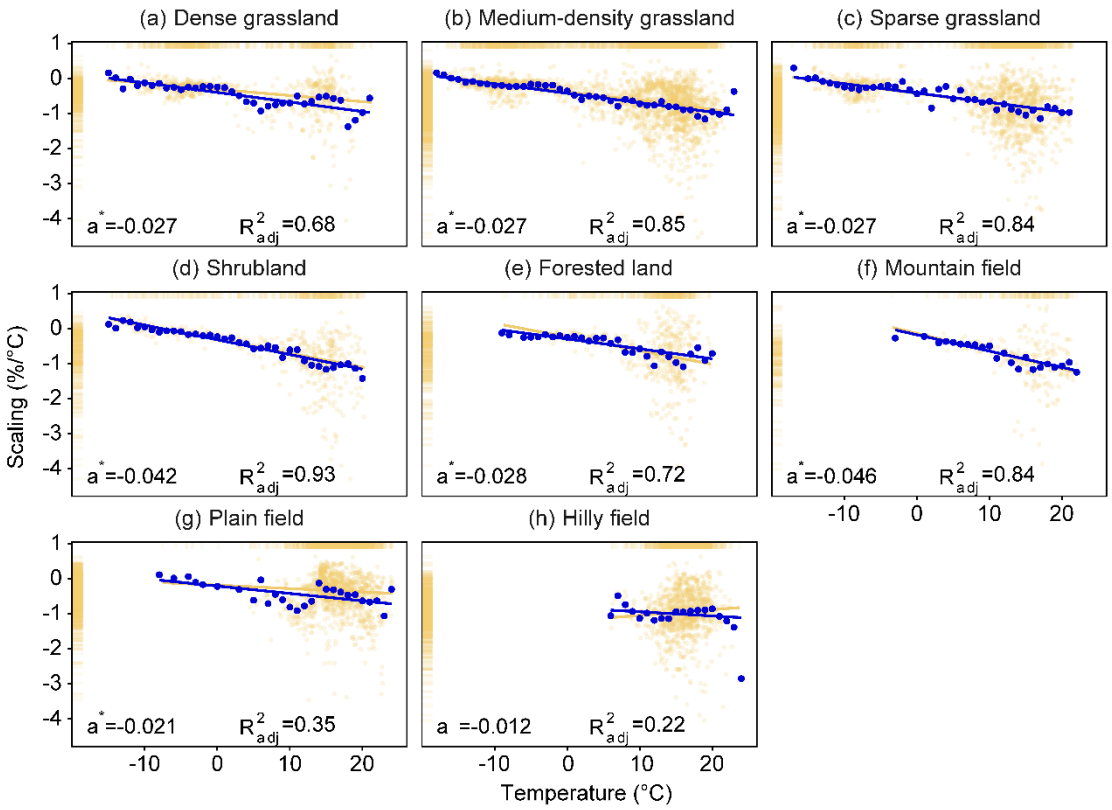

Figure 7. Scatter plot of scaling with temperature. Orange points with transparency indicate the SSM-Temperature scaling (y-axis) versus the multi-annual average temperature (x-axis) for each grid cell in the Yellow River Basin. Blue points indicate the temperature versus the scaling averaged for every 1 ºC interval of temperature for all grid cells. The adjusted R square and coefficient of quantile regression are provided for each land cover type (showing the scaling and temperature have a strong relationship for most land covers). Asterisks (*) indicate that the linear regression is significant ($p<0.05$).

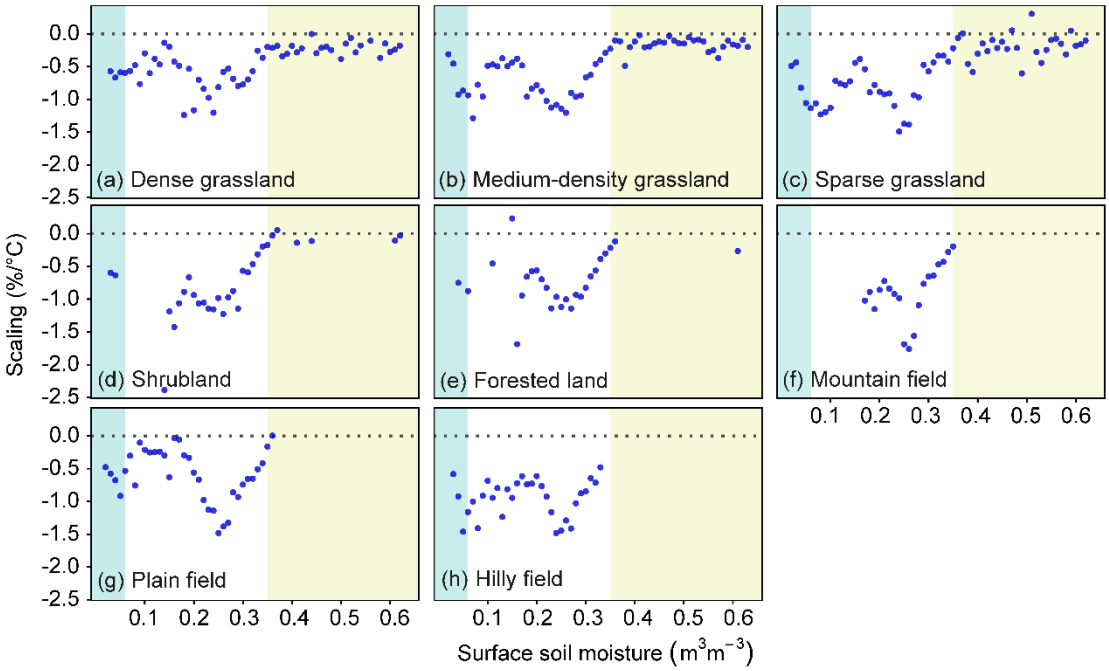

Figure 8. Scatter plot of scaling with SSM. Points indicate the multi-annual average SSM (x-axis) versus the SSM-Temperature scaling (y-axis) averaged for every 0.01 m^3m^{-3} interval of surface soil moisture for all grid cells. The colored backgrounds indicate two critical values: the lower and upper critical values, respectively.